Journal of Vibration Engineering & Technologies (2026) 14:230
https://doi.org/10.1007/s42417-026-02463-2

ORIGINAL PAPER

Role of Friction in Vibro-Impacts and Machining Stability of Impact-Damped Boring Bars

Arjun Patel[1] · Mohit Law[1] · Pankaj Wahi[1]

Received: 10 November 2025 / Revised: 30 March 2026 / Accepted: 1 April 2026

Abstract

Purpose In an impact-damped boring bar, the momentum transfer from the vibrating bar to a free mass colliding with it damps the bar's response. For effective momentum transfer, the free mass within the bar must slide/roll from one side to the other by overcoming frictional resistance. Despite its importance, the role of friction remains insufficiently unexplored. This paper hence presents research that examines the role of friction on the nature of vibro-impacts influencing instabilities in the boring process.

Methods We present model-based parametric analysis in which the bar is modelled as a cantilevered beam and the free mass is taken as a ball that slides/rolls over the contacting surface. Frictional interactions are considered. The governing nonlinear equations are solved numerically to evaluate performance under harmonic and regenerative cutting forces.

Results We observe the nature of vibro-impacts to be strongly dependent on friction, on the excitation level, the excitation frequency, the gap between the free mass and the walls of the bar, on ratio of the free mass to the modal mass of the boring bar, and on the initial conditions. Families of solutions for vibro-impacts include multiple symmetric and asymmetric impact cases, no impact cases, as well as cases with ball sticking to a wall and cases with the ball exhibiting non-uniform modulated response. Sensitivity analyses indicate that the vibro-impact responses are largely robust to variations in initial conditions, except for the no impact motion under harmonic forcing. When friction is considered, multiple attractors with different vibration amplitudes may coexist depending on the harmonic forcing amplitude. While changes in mass ratio and friction coefficient significantly influence system stability, variations in the coefficient of restitution have negligible effects on the response characteristics.

Conclusions Our analysis reveals that friction changes the nature of vibro-impacts resulting in a transition of response from one solution type to others. We also in general observe that friction retards motion of the free mass and hence inhibits its ability for effective momentum transfer. Future work should extend these insights experimentally to validate transition phenomena and quantify frictional effects under realistic surface conditions.

Keywords Impact damper · Friction · Boring bar · Vibro-impacts · Machining instability · Chatter

Introduction

Machining deep bores requires the use of slender, high-aspect ratio cantilevered boring bars. These tools tend to vibrate when excited by the cutting process. Since vibrations deteriorate machined surface quality, they must be damped. Damping is usually achieved by integrating a tuned mass damper within the boring bar, or by active vibration control that requires a sensor and actuator to be integrated within the boring bar [1]. As an alternative to these solutions, this paper focuses on characterizing the dynamics of an impact-damped boring bar to evaluate its damping potential.

Impact dampers include a free mass that collides with the vibrating tool. The ensuing momentum exchange transfers energy from the primary system to the free mass, thus minimizing the primary system's vibratory response. Impact dampers are purported to be simpler and robust to changes in operating conditions, and as such the dynamics of impact-damped boring bars have been investigated by others [2–7]. Seminal amongst those is the report by

✉ Mohit Law
mlaw@iitk.ac.in

[1] Department of Mechanical Engineering, Indian Institute of Technology Kanpur, Kanpur 208016, India

Thomas et al. [2]. Though they showed the impact damper to be effective, their design and analysis were for an impacting mass that was not free but was supported in soft springs. Their system was hence one in which the impacting mass could also behave as a potentially (de)tuned vibration absorber, making it difficult to isolate the influence of the impact damper from that of an absorber. A similar hybrid concept was also investigated in a more recent study [5]. Another significant experimental report on an impact damper was by Ema and Marui [3], in which the impacting mass was placed outside of the boring bar. Recent related investigations reported in [4] and by the author's research group also explored a similar concept using an external/ring damper [6]. Since placing the damper outside reduces the effective working length of the boring bar, such [3, 4, 6] solutions are not practical.

In contrast to earlier approaches to impact-damped tools, which were either hybrid or externally configured and hence impractical, this work focuses on the only viable solution: embedding the free mass within an internal cavity of the boring bar. Since the free mass is to be placed within the bar, for effective momentum transfer, it must slide/roll from one side to the other to impact the side walls on either side. When sliding/rolling, it must overcome frictional resistance at the contacting surface. Since friction is likely to govern the performance of an impact-damped tool, the main aim and new contribution of this paper is to examine the role of friction on the nature of vibro-impacts. Beyond friction, the study also characterizes performance as influenced by the clearance between the free mass and the cavity walls, the excitation amplitude and frequency, and the ratio of the free mass to the modal mass of the boring bar. These parameters have been consistently identified as critical determinants in impact-damped systems [8–12], and yet, their role has not been examined in impact damped boring bars. This is something we will address and remedy.

The boring bar with an impact damper integrated within it and subject to cutting process-based excitations is akin to a periodically forced system with a constraint that leads to motions with impacts between the free mass and the tool. Such systems are known to behave like nonlinear and chaotic devices [4, 13]. Hence, to fully understand response, we investigate the system being separately subjected to harmonic and regenerative cutting force-based excitations. Our investigations about the potential of impact-damped tools to mitigate machining instabilities due to regenerative effects are the first such report and may be considered to be the second novel contribution of this research.

To demonstrate the workings of the system, we present model-based parametric analysis in this paper. In our model, the bar is modelled as a cantilevered beam, and the free mass is taken as a ball that slides/rolls over the contacting surface. Using a beam model allows us to integrate the cavity (inside of which the free mass is to be placed) within the bar to be anywhere within the bar. Moreover, the beam model also allows us to apply forces at the free end of the bar, which is also the cutting end and track interactions between the free mass and the bar at locations where those interactions take place. This approach overcomes the limitations of other classical modeling approaches that approximate the primary system as a single degree of freedom model – in which the forced excitation and interactions between the free mass and the primary system were constrained to the same location, something that is not physically correct. We approximate the interactions between the free mass and the bar as partially elastic collisions using an appropriate coefficient of restitution (COR). Since the COR approach requires its selection from a database, it makes modelling simpler than approximating the interaction interface with spring and damper connections, parameters of which must be tuned appropriately [7, 10]. The resulting governing nonlinear equations are solved numerically to evaluate performance under harmonic and regenerative cutting forces. To benchmark the damping potential of the impact-damped boring bar, we also compare its performance with that of a boring bar integrated with a tuned mass damper tuned using the classical Den-Hartog method [14, 15]. However, if other optimization criteria, such as the Sims [16] equal-real-trough method, are used for tuning, the damping performance of the TMD can improve further, enabling it to outperform both the Den Hartog-tuned absorber and the impact damper.

Note that our investigations are limited to one free rigid spherical mass impacting a boring bar. There are also reports on the use of particle dampers in boring bars. Since particle dampers work very differently from impact dampers, they do not form the focus of this study. Moreover, though cutting process-based excitation acts in all three directions—along the cutting velocity, feed, and radial directions, since the force along the cutting velocity direction does not contribute to the regeneration of chip thickness [17], and since the bar is stiff along its feed direction, for the analysis herein, we only consider impacts, flexibility and regeneration in the radial direction.

The remainder of the paper is organized as follows. The section titled 'Modelling vibro-impacts' presents the model. Numerical results for harmonic excitation are reported in the section titled 'Vibro-impacts under harmonic excitations'. Machining instabilities are examined in the 'Stability analysis' section. In the 'Discussions' section, we discuss the role of changing mass ratio, changing initial conditions, and changes due to other important parameters. That analysis is followed by the main conclusions.

Modelling Vibro-Impacts in an Impact Damped Boring Bar

A design concept of a cantilevered boring bar with an impacting free mass is illustrated in Fig. 1(a). The bar is assumed to have a diameter D of 25 mm and length L of 200 mm, i.e., a L/D of 8. The bar has a cavity drilled across its diameter at a distance a_1 of 122 mm from the free end to accommodate a free mass. The free mass is a spherical ball of mass m and diameter d of 15 mm positioned within the cavity as near the cutting end as possible. The side plugs shown retain the free mass within the cavity and their thickness can be adjusted such as to adjust the gap, δ. The bar has a cartridge at the free end for holding the cutting insert, which is attached to the main body through an end plug, while the opposite end is fixed in the clamping holder.

Due to geometric non-uniformities along its length on account of the cavity and the cartridge, the bar is divided into four distinct sections for modelling purposes, as illustrated in Fig. 1(b). Section 1 of the beam that extends from the fixed end to a distance a_1 is assumed to be solid with a constant diameter. Section 2 that spans from a_1 to a_2 is 15.1 mm wide, i.e., just wider than the diameter of the ball. And since this section has a cross-drilled hole, its diameter varies along the length of this section. Hence, for the purpose of modelling, we assume a diameter of 17 mm. The remainder is made up by the side plugs, which for modelling purposes, are assumed massless. The side plugs allow for a maximum gap of 1 mm on either side of the ball when the ball is in the middle of the cavity. Section 3 that represents the end plug has a uniform diameter of 22 mm and extends from a_2 to a_3 and has a width of 32.9 mm. Section 4 represents the cartridge, whose geometry is nonuniform; therefore, an equivalent diameter of 19 mm is adopted to account for its mass and stiffness contributions in the beam model. The bar is assumed to be made of steel, with material properties defined as: Young's Modulus (E) of 200 GPa, and mass density (ρ) of 7850 kg/m^3. Cutting forces are assumed to act at the free (cutting) end and only in the $X-$ direction, i.e., the radial direction. Accordingly, only radial vibratory motion is considered in the analysis. The weight of the ball is neglected since gravity acts in the positive $Y-$ direction.

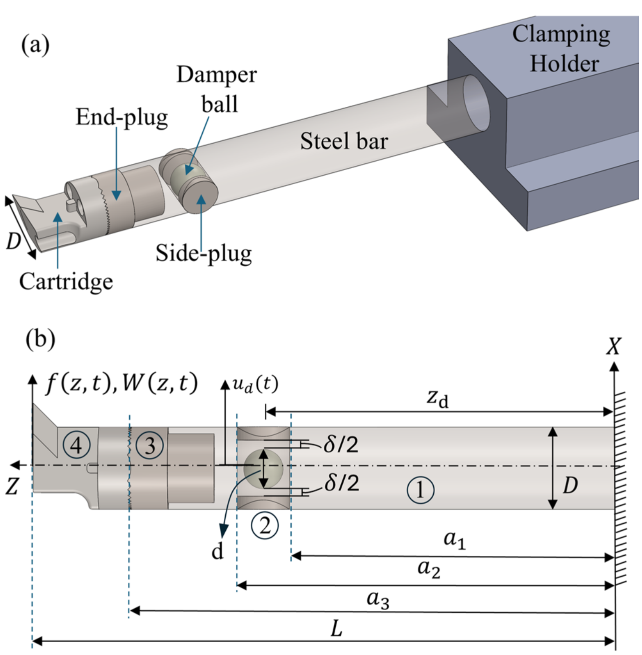

Fig. 1 (**a**) Design concept of an impact-damped boring bar, (**b**) schematic for modelling the system shown in (a)

The motion of the bar at the free end is $W(z,t)$. Motion of the ball is $u_\mathrm{d}(t)$. And motion of the bar at the impacting location is $W(z_\mathrm{d},t)$. When the relative displacement between the ball and the bar exceeds the available clearance, the ball impacts the inner walls (side plugs) of the cavity. Mathematically, impacts occur when $u_\mathrm{d}(t) - W(z_\mathrm{d},t) = \pm\,\delta/2$, wherein δ is the total gap between the side plugs and the ball.

Modelling the bar using the Euler-Bernoulli beam theory, the governing equations of motion describing the boring bar and the damper can be shown to be:

$$\rho A\frac{\partial^2 W(z,t)}{\partial t^2} + \frac{C}{L}\frac{\partial W(z,t)}{\partial t} + EI\frac{\partial^4 W(z,t)}{\partial z^4} = f(L,t) - F_\mathrm{rf}(z_\mathrm{d}), \quad (1)$$

$$m\ddot{u}_d(t) = F_\mathrm{rf}, \quad (2)$$

wherein the three terms on the left hand side in Eq. (1) denote the forces derived from the kinetic, damping, and potential energy of the beam and wherein ρ, A, C, E, and I represent the mass density, cross-sectional area, damping coefficient, Young's modulus, and area moment of inertia of the beam, respectively. All these parameters are functions of z to account for variations in geometrical properties along the beam. The term F_rf denotes the friction force acting between the impacting ball and the bottom surface of the cavity along which it rolls. Equation (2) is a force balance between the acceleration force of the impacting mass and the frictional force resisting its motion.

The term $f(L,t)$ denotes the external force acting at the free end of the beam. If harmonic, the forcing function becomes: $f(L,t) = F_0\sin(\Omega t)$, wherein F_0 is the magnitude of external forcing and Ω is the excitation frequency. Whereas, if forces are of the regenerative type then, in that case the forcing function becomes [18]:

$f(L,t) = K_\mathrm{r}bh$, wherein K_r is the radial cutting force coefficient, b is the depth of cut, h is the instantaneous chip thickness. The instantaneous chip thickness considering the regenerative effect can be expressed as:

$h = h_\mathrm{m} + W(L,t-\tau) - W(L,t)$, wherein h_m is the mean chip thickness, τ is the time period corresponding to one spindle revolution, $W(L,t)$ is the bar's tip displacement at time t, and $W(L,t-\tau)$ is the bar's tip displacement in the previous revolution. During machining, h can depend not only on the current tool vibration and the vibration from the previous revolution, but also on vibrations from two or more earlier revolutions. Therefore, to account for the net effect of vibration on the chip thickness, the minimum of $\{h_{\mathrm{m}} + W(L,t-\tau),\ 2h_{\mathrm{m}} + W(L,t-2\tau),\ 3h_{\mathrm{m}} + W(L,t-3\tau),\ldots,\ Nh_{\mathrm{m}} + W(L,t-N\tau)\}$ is considered, wherein N is the total number of spindle revolutions assumed in the analysis. Dependence of h on multiple previous revolutions can result in a negative value during analysis, indicating that the tool is not engaged in cutting, and that it is out of the cut due to the large amplitude of ensuing vibrations. At such time instances, h is to be set to zero in the simulation. The chip thickness and the force going instantaneously to zero are also the conditions to classify that case as a case of unstable chatter vibrations.

The frictional force term in Eqs. (1)–(2), can be expressed with a dry (Coulomb) friction model [19]:

$$F_{\mathrm{rf}} = \frac{1}{r_{\mathrm{m}}}\nu_{\mathrm{rf}} mg\left(\mathrm{sgn}(\dot{y})\right); \mathrm{sgn}(\dot{y}) = \begin{cases} 1, & \dot{y} > 0; \\ 0, & \dot{y} = 0; \\ -1, & \dot{y} < 0, \end{cases} \tag{3}$$

wherein r_{m} is the radius of the ball, ν_{rf} is the coefficient of dynamic friction, and g is the acceleration constant due to gravity. Although the frictional force is modeled here using Coulomb's friction law, the coefficient ν_{rf} is treated as a dimensional parameter that depends on the ball radius r_{m}. And, in that sense, sticking is not considered and a pure sliding (Coulomb) friction formulation is adopted; accordingly, the friction force is expressed using the sign of the relative velocity in Eq. (3), which is akin to a sliding friction force.

The relative displacement $y(t)$ is defined as the displacement of the damper mass relative to the boring bar at the damper location along the transverse vibration direction, i.e., $y(t) = u_{\mathrm{d}}(t) - W(z_{\mathrm{d}},t)$. Here, $u_{\mathrm{d}}(t)$ denotes the displacement of the damper mass and $W(z_{\mathrm{d}},t)$ represents the displacement of the boring bar at the damper location z_{d}. $\dot{y}$ is the relative velocity between the ball and bar, which is obtained from solving for displacement. To determine the displacement of the bar, the response $W(z,t)$ is expressed as the superposition of all modeshapes of the beam: $W(z,t) = \sum_i u_i(t)\psi_{\gamma i}(z)$, wherein $u_i(t)$ is the temporal component of beam displacement, wherein $\psi_{\gamma i}(z)$ denotes the modeshapes or eigenvectors of the beam, γ designates the section of the beam assumed, i.e., 1, 2, 3, and 4, and i denotes the number of modes.

By applying the orthogonality property of the modes, and limiting analysis to only the first and dominant mode of the beam, the reduced and modified governing equation of motion for the bar can be shown to become:

$$M\ddot{u} + C_L\dot{u} + Ku = f(L,t)\psi_{\gamma 1}(L) - F_{\mathrm{rf}}\psi_{\gamma 1}(z_{\mathrm{d}}), \tag{4}$$

wherein $M = \int_0^L \rho_\gamma A_\gamma \psi_{\gamma 1}\psi_{\gamma 1} dz$, $C_L = \frac{C}{L}\int_0^L \psi_{\gamma 1}\psi_{\gamma 1} dz$ and $K = E_\gamma I_\gamma \beta_n^4 \int_0^L \psi_{\gamma 1}\psi_{\gamma 1} dz$. The β_n^4 within K is given as $\rho_\gamma A_\gamma \omega_n^2 / E_\gamma I_\gamma$, wherein ω_n is the natural frequency of the beam. C_L denotes the damping coefficient per unit length representing distributed viscous damping proportional to the local transverse velocity, and its value in Eq. (4) is evaluated by assuming a damping ratio of 0.01. M and K represent the generalized modal mass and stiffness of the first mode obtained from the distributed beam model based on the known geometry and material properties, while the corresponding mode shapes are determined by solving the eigenvalue problem of the discretized Euler–Bernoulli cantilever beam model.

The vibrating boring bar, when subjected to external excitation, induces oscillatory motion of the ball and repeated collisions. These impacts introduce discontinuities in the relative velocity of the system and, together with the effects of friction, render the governing equations nonlinear. Therefore, to account for the influence of the ball on the bar's dynamics, Eq. (2) and Eq. (4) are numerically integrated using the fourth-order Runge-Kutta method. At each time step, the impact condition is tested. Whenever an impact occurs, the velocities of both the bar and the ball are updated. The post-impact velocities are determined using the principles of linear momentum conservation and the COR. The linear momentum balance between the bar and the ball, applied immediately before and after the impact, is expressed as:

$$\begin{aligned} &M\dot{u}_-\psi_{\gamma 1}(z_{\mathrm{d}}) + m\left(\dot{y}_- + \dot{u}_-\psi_{\gamma 1}(z_{\mathrm{d}})\right) = \\ &M\dot{u}_+\psi_{\gamma 1}(z_{\mathrm{d}}) + m\left(\dot{y}_+ + \dot{u}_+\psi_{\gamma 1}(z_{\mathrm{d}})\right), \end{aligned} \tag{5}$$

wherein subscripts '$-$' and '$+$' are the instants just before and after the impacts. The COR, denoted as e is defined as:

$$\dot{u}_+\psi_{\gamma 1}(z_{\mathrm{d}}) - \left(\dot{y}_+ + \dot{u}_+\psi_{\gamma 1}(z_{\mathrm{d}})\right) = -e\left(\dot{u}_-\psi_{\gamma 1}(z_{\mathrm{d}}) - \left(\dot{y}_- + \dot{u}_-\psi_{\gamma 1}(z_{\mathrm{d}})\right)\right). \tag{6}$$

On solving Eqs. (5–6), The velocity of the bar and the relative velocity after the impact yield:

$$\dot{u}_+ = \dot{u}_- - \frac{\mu(1+e)}{(1+\mu)\psi_{21}(z_{\mathrm{d}})}\dot{y}_-; \dot{y}_+ = -e\dot{y}_-, \tag{7}$$

wherein μ is the mass ratio defined as the ratio of the mass of the ball to the modal mass of the boring bar.

After each impact, the bar velocity and relative velocity are updated using Eq. (7), and numerical integration proceeds in the next time step with these updated values. In this manner, the complete displacement and velocity profiles of both the bar and the ball are computed throughout the simulation with the help of Eqs. (2), (4) and (7). For the numerical integration, we use a time step of 10^{-6} seconds and let the solution run for a total duration of 2 s. This time step is several orders of magnitude smaller than the period of vibration and as such the solutions obtained are numerically stable. Note that the motion is not divided into separate regimes such as free flight, sticking, or sliding. Instead, the dynamics are computed continuously, and the transitions between contact and separation arise naturally from the impact constraints without introducing additional switching rules or special termination criteria for Zeno-type impact sequences.

Having presented the model for an impact-damped boring bar, we evaluate its damping and stabilizing potential by assessing its performance separately under harmonic and regenerative excitations as discussed in the next sections. For all analyses, we assume the free mass to be made of carbide. For a 15 mm diameter, its mass is evaluated to be 26 g. The friction coefficient between the ball and steel bar is taken to be 0.6 mm [19]. And, the COR for carbide impacting the steel bar is taken to 0.7 [20]. We present analysis for two representative gap values – 0.1 mm and 0.5 mm. To benchmark performance of the impact-damper with a tuned mass damper, we base the tuned-mass damper design on [15, 21]. For which the bar is assumed to have a cavity that is 80 mm in length and 21 mm in diameter. This will accommodate a carbide absorber of 80 mm length and 20 mm diameter. The absorber mass is assumed to be supported in a spring-damper combination, parameters of which are estimated using the classical Den Hartog's method [14].

Vibro-Impacts under Harmonic Excitation

We analyze response of the bar under two levels of excitation forces – 10 N and 20 N. These values correspond to the typically expected oscillatory component of cutting forces for assumed cutting of Aluminium (K_{r} = 850 MPa) with a feed of 0.1 mm/rev, and a depth of cut ranging from 0.1 to 0.2 mm. Note that we ignore the DC component of the force. For the given size, material and geometry of the bar, the first natural frequency of the solid bar was evaluated to be 456 Hz. For the bar with a cavity that houses a free mass, the natural frequency was 461 Hz. We evaluate vibro-impacts for forcing frequencies in this neighborhood, i.e., when the ratio of the forcing frequency to the natural frequency of the respective bars varied from 0.95 to 1.05 in increments of 0.01. The performance of the boring bar is assessed by computing the root mean square (RMS) value of the displacement at the cutting end. For analysis herein, we take the bar and the ball to be stationary at time, $t = 0$ and also assume the ball is centered in the cavity at the start of simulations. The influence of changing initial conditions and a change in the free mass is presented in the 'Discussions' section. To eliminate the effect of initial transients, the RMS displacement is calculated after discarding the first 20% of the time-history data for each case. The expression used for the RMS calculation is given as follows:

$$RMS = \sqrt{\frac{1}{N}\sum\ {}_{i=1}^{N}(u_i\,(t)\,\psi_{\,41}\,(L))^2}; \tag{8}$$

wherein $u\,(t)$ denotes the generalized displacement of the boring bar, $\psi_{\,41}\,(L)$ represents the value of corresponding eigenfunction at the tool tip, wherein L is the length of bar measured from the clamped end, and N is the number of data samples.

Figure 2 shows the RMS displacements for the force being low at 10 N, and Fig. 3 shows response for the high force level of 20 N. In both figures, we show subplots for different levels of gaps. For each force and gap level, we also show separate subplots for how the response changes with and without friction in the model. In each figure, we also show representative cases of the relative displacements between the bar and ball to reveal the nature of vibro-impacts being governed by the excitation frequency, as well as the gap and friction. The figures also show the response obtained with the tuned mass damper, for which the absorber mass, stiffness, and damping were evaluated to be 0.39 kg, 1.05 MN/m, and 505 N-s/m, respectively.

As is evident from Fig. 2, when the excitation frequency equals the natural frequency, i.e., at resonance, the response of the solid bar without the damper is highest. The behavior below and above resonance for this case is consistent with response expected of single degree of freedom systems. Expectedly, this response is not governed by a change in gap or by friction. Likewise, the response of the tuned mass damped system is also independent of friction and gaps. The RMS displacement of the tuned mass system, when compared to a boring bar without damper shows a reduction of approximately 88% at resonance. Although the RMS response of the TMD varies slightly, the variation between its maximum and minimum values is very small. When plotted together with the solid bar response, whose maximum RMS value is approximately 8.7 times larger, the RMS response of the TMD appears nearly flat.

For the case of the impact damper, Fig. 2 reveals that the ball can exhibit a variety of impact patterns and that there is a strong dependence of the nature of vibro-impacts on the forcing frequencies. For example, for the gap being 0.5 mm and when friction is ignored, Fig. 2(a) reveals that there can be two types of solutions: no impacts and non-uniform impacts. The relative displacement for the no-impacts case

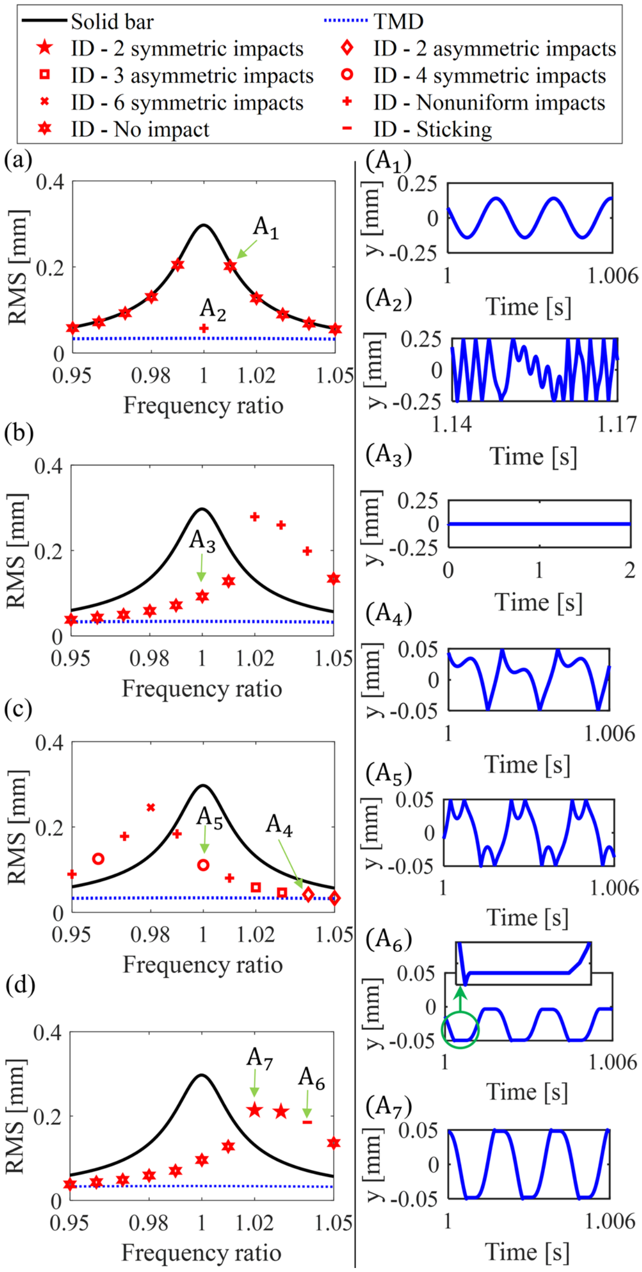

Fig. 2 RMS displacement at the cutting end of the bar under a 10 N harmonic force for a solid bar, a bar with a tuned mass damper (TMD), and a bar with an impact damper having gaps of **(a)** 0.5 mm without friction, **(b)** 0.5 mm with friction, **(c)** 0.1 mm without friction, and **(d)** 0.1 mm with friction (left column). The right column shows the relative displacement response corresponding to various impact patterns: A_1- No impact, A_2- Nonuniform impact, A_3- No impact (with sticking), A_4- 2-asymmetric impact, A_5- 4-symmetric impact, A_6- Sticking, and A_7- 2-symmetric impact (with sticking)

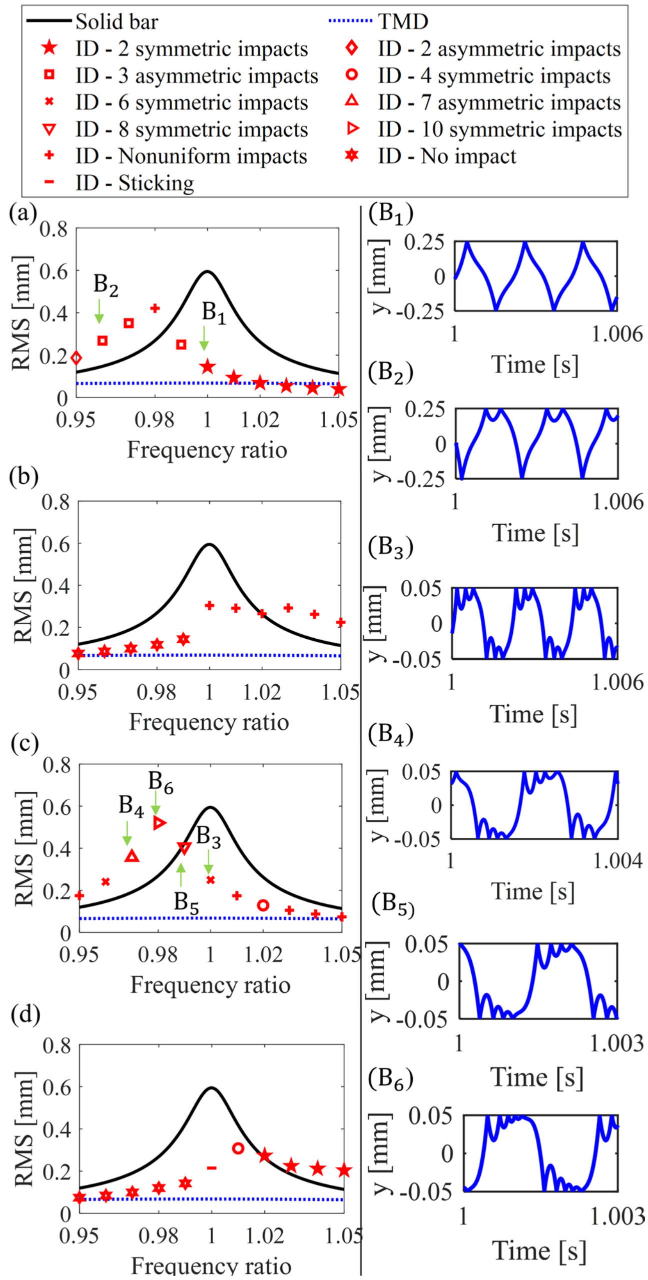

Fig. 3 RMS displacement at the cutting end of the bar under a 20 N harmonic force for a solid bar, a bar with a tuned mass damper (TMD), and a bar with an impact damper having gaps of **(a)** 0.5 mm without friction, **(b)** 0.5 mm with friction, **(c)** 0.1 mm without friction, and **(d)** 0.1 mm with friction (left column). The right column shows the relative displacement response corresponding to various impact patterns: B_1- 2-symmetric impact, B_2- 3-asymmetric impact, B_3- 6-symmetric impact, B_4- 7-asymmetric impact, B_5- 8-symmetric impact, and B_6- 10-symmetric impact

is shown as case A_1. And as evident therein, $y < \delta/2$, and hence there are no impacts. Since there are no impacts, there is no improvement in the impact-damped bar's response in comparison to the response of the solid bar. This holds true for all other such cases of no impacts. For the other case of non-uniform impacts, shown as A_2, the relative displacement appears to transition from uniform impacts on either side ($y \geq \delta/2$) to no impacts and then back to the case of uniform impacts. The impacts, even if non-uniform, clearly transfer momentum from the bar to the ball. The RMS displacement for this case is 0.057 mm, which is approximately 80% lower than the response of the solid bar, and almost the same level as that of the improvement with the tuned mass system.

When friction is included in the model for the same gap of 0.5 mm, though the response appears to right-shift – as is evident in Fig. 2(b), the vibro-impacts are of the same two types as the case without friction, i.e., no impacts and non-uniform impacts. The non-uniform case of impacts is like the response shown in A_2. The case of no impacts is however different. The response for one representative case A_3 shows the relative displacement to be approximately zero, i.e., $y \cong 0$. This suggests that the ball and bar are moving out of phase, such that their relative motion cancels each other out. Interestingly, for cases of no impact at several frequency ratios, the RMS values for the impact-damped bar's response are lower than the response of the solid bar, and as damped as the response is for the case of the tuned mass system, especially at lower frequency ratios. One possible explanation for this is that friction results in the ball sticking to the bottom surface with potential microslip motion, which continuously dissipates the bar's vibrational energy by converting mechanical energy into heat [22–24]. Furthermore, when the damper mass sticks to the bar, the effective modal mass of the system increases due to the inclusion of the 26 g damper mass, leading to a slight reduction in the natural frequency from about 461 Hz to approximately 452 Hz. However, since the effect of this change in natural frequency on the system response has not been separately isolated, it cannot be concluded with certainty whether it influences the observed frequency response characteristics. Moreover, because sticking can be a transient phenomenon and its influence may depend on parameters such as gap and coefficient of friction, a detailed investigation is left for future work. All cases of non-uniform vibro-impacts result in the impact-damped boring bar performing worse than the solid boring bar. This suggests that vibration reduction with impact-damped systems is not guaranteed, and that impact-dampers may amplify response instead of damping it if operating parameters are not chosen correctly. These observations agree with reports in the literature [2, 8], despite those reports not factoring the influence of friction in their analysis. Moreover, the right-shift observed in RMS response characteristics also agrees with base-excitation impact-damped experiments reported in [25]. In those experiments motion of the ball was tracked using vision-based methods, and the ball was indeed observed to roll from one side to the other. This suggests that ball rolling and friction could indeed cause a right-shift in response as is predicted by our model-based analysis.

For the case of the gap being 0.5 mm gap and friction being ignored, the ball exhibits impacts only at the resonant frequency. The behaviour changes significantly when the gap is reduced to 0.1 mm – see Fig. 2(c). There are five types of vibro-impacts in this case. These range from non-uniform impacts to two and three asymmetric impacts per cycle of motion of the bar, and cases of four and six symmetric impacts. Nature of the vibro-impacts changes with changing frequency ratios. The RMS trend in Fig. 2(c) shows a noticeable leftward shift relative to the solid bar, indicating a change in resonance behavior when friction is not included in the model. A similar observation was reported by Masri [8] where an impact damper undergoing two symmetric impacts exhibited a leftward shift in the peak of the damped response in one case, while in another, the response was found to be independent of the forcing frequency. In contrast, Fig. 2 highlights a strong dependence on the forcing frequency and a lack of consistency in the observed impact patterns. Furthermore, although the RMS frequency response appears symmetric about frequency ratio (r) of 0.98, the corresponding time-series responses of the bar and the ball are not exactly identical.

As representative examples of the impact damped response for the gap being 0.1 mm and friction being ignored, we show the relative displacements for two cases: the two-asymmetric impacts case (A_4) and the four-symmetric impacts case (A_5). Unlike the two-symmetric impact case, where impacts occur exactly half a cycle apart, in the two-asymmetric impact case, the second impact may occur slightly before or after π/Ω if the first occurs at time zero. The damping performance of the A_4 case demonstrates an effectiveness comparable to that of a tuned mass system. This result is consistent with findings in prior studies where properly phased asymmetric impacts were shown to achieve significant vibration attenuation [8]. At resonance, the ball experiences four impacts per cycle, two impacts on either side wall – as is evident from the relative displacements shown in A_5. The RMS displacement of the bar reaches 0.11 mm, i.e., a reduction of approximately 63% in comparison to the response of the solid boring bar. This reduction is less than the case of the gap being 0.5 mm. This result indicates that even in cases where the bar's response exhibits strong modulation with non-uniform impacts and no steady state (as it was for the higher gap of 0.5 mm), the performance surpasses that of symmetric steady-state responses.

The inclusion of friction with a 0.1 mm gap suggests vibro-impacts of three types: no-impacts, two-symmetric impacts, and ball sticking. The right-shift in the RMS response is like that was observed for the case of the gap being 0.5 mm. The shift can hence be attributed to the same rolling and friction phenomenon. Likewise, the impact-damped response with a lower gap at lower frequency ratios being compared to the tuned mass system's response is consistent with the impact-damped response observed for the gap being 0.5 mm. Of the three types of vibro-impacts observed, the no-impacts case is like the A_3 case. Hence, we show the relative displacements for the two other cases, namely sticking and two-symmetric cases, denoted as A_6 and A_7..

As seen in the relative displacement plot of A_6, the ball impacts one side of the cavity wall and separates immediately after impact; however, it sticks slightly away from the sidewall, as indicated by the constant relative displacement shown in the inset. The relative displacement plot of A_6 shows a flat line twice per cycle, near zero, and once near half of the total gap, slightly offset in both cases, suggesting that sticking occurs twice in each cycle of the bar's motion. This sticking behavior resembles that of the case A_3, where sticking persists throughout the simulation without any impacts, leading to its classification as a no-impact case. In contrast, the sticking in A_6 is of shorter duration and is classified as a sticking case, since the ball also impacts one side of the cavity wall. Since the ball is initially placed at the center of the cavity in the simulation, the relative displacement reaches a constant value approximately equal to half the gap during sticking near the sidewalls, whereas it approaches zero when the ball is stuck near the center. The occurrence of two sticking events per cycle leads to stick–slip behavior, contributing to energy dissipation. However, this case performs worse than the solid bar and no-impact cases, suggesting that energy dissipation through dry friction is less effective than continuous sticking throughout the motion.

The relative displacement plot of A_7 shows two symmetric impacts per cycle; however, sticking also persists, similar to that observed in the inset of A_6. Although prior research has reported that two-symmetric impacts per cycle result in the most effective damping, our analysis reveals that in the presence of friction, these impacts are accompanied by partial sticking in each cycle. In this case, the damper mass may temporarily transfer its stored kinetic energy back to the structure, resulting in a local increase in vibration amplitude, and as such, the response with vibro-impacts is larger than even the solid bar.

We next discuss the nature of vibro-impacts when the force level is increased to 20 N. Response for this case is shown in Fig. 3. As expected, the response of the solid bar increases in proportion to the increase in force levels. The response of the tuned mass system also scales proportionally as the excitation force magnitude is doubled, which is expected. In contrast to the solid bar's response and the tuned mass system's response, since vibro-impacts are nonlinear they do not follow response characteristics as were seen in Fig. 2 for the lower force level of 10 N. Interestingly however, for the higher force level, the leftward shift in the RMS trends for without friction and the rightward shift with friction is consistent with observations for the lower force level. In this case too, the nature of vibro-impacts is found to be strongly dependent on the frequency ratio, on gaps, and on friction.

For the higher gap of 0.5 mm, when friction is ignored, the response is shown in Fig. 3(a). Unlike the case for the lower force level (see Fig. 2(a)), where impacts occurred only at resonance, a different behavior is observed. In this case, four types of vibro-impacts appear: two symmetric impacts, two and three asymmetric impacts, and non-uniform impacts. Since we have already discussed what non-uniform impacts and two asymmetric impacts look like in Fig. 2, we show herein representative cases of what the other two impacts are like. At resonance, we observe there to be two symmetric impacts – see the relative displacements shown in B_1, wherein $y \geq \delta/2$ is clearly evident. The reduction in the RMS level at resonance is approximately 85% compared to that of the solid bar. Though this is significant, it is still less than the reduction possible with the tuned mass system. However, at higher excitation frequencies, the impact damper performs comparably to, and in some instances better than, the tuned mass damper. These observations are consistent with previous reports, which suggest that the two symmetric impacts per cycle is the preferred vibro-impacting nature for energy absorption from the primary system [9, 11, 26]. The other case for which we show representative three-asymmetric impacts per cycle corresponds to the response at a frequency ratio below resonance. The relative displacement of B_2 shows that it reaches half the gap twice on one side of the cavity, resulting in two impacts with that wall, and once on the opposite side, resulting in a single impact there during each cycle. In this case as well, the damper mass may temporarily transfer its stored kinetic energy back to the structure, resulting in a local increase in vibration amplitude. Three asymmetric impacts faring worse than two symmetric impacts was also observed in base excitation impact-damped experiments reported in [11]. However, our analysis also suggests that, depending on the excitation and gap size, even three-asymmetric impacts can perform comparably to a tuned mass damper, as seen in Fig. 2(c).

When friction is included in the model, for when the gap and force levels are high, the nature of vibro-impacts changes as shown in Fig. 3(b) in comparison to friction being ignored. There are now two types of behavior: no impacts and non-uniform impacts. And, like for the lower force level, in this case too, the case of no-impacts results in reduction in RMS levels in comparison to the solid boring bar. A possible reason for this reduction is friction resulting in the ball sticking to the bottom surface with potential microslip motion, which continuously dissipates the bar's vibrational energy. The cases of non-uniform vibro-impacts result in mixed behavior. At resonance, nonuniform impacts lead to a reduction in the RMS levels of the bar compared to the solid bar. However, at higher frequency ratios, the RMS levels become amplified compared to the solid bar due to the combined effects of friction and nonuniform impacts. Since the relative displacements for these two cases (no impacts and non-uniform impacts) are already shown in Fig. 2, they are not shown again in Fig. 3.

The RMS response for the 0.1 mm gap without friction and force being high is shown in Fig. 3(c). And, as is evident, there are six different types of vibro-impacts observed. These include cases of non-uniform impacts and cases of multiple symmetric and asymmetric impacts. In general, there appears to be a higher number of impacts per cycle compared to the case with a lower force level that was shown in Fig. 2(c). The higher number of impacts can be explained by the increase in the bar response due to the higher force level, while the gap remains small [22]. The relative displacements of four different impact patterns are presented in the right column of Fig. 3. Cases B_3, B_5, B_6 and B_4 correspond to six, eight, and ten-symmetric impacts per cycle, and seven-asymmetric impacts per cycle, respectively. Their relative displacement plots illustrate distinct impact patterns. Figure 3(c) shows that these increased numbers of impacts result in RMS amplitudes that are either similar to or worse than those of the solid bar. However, at higher excitation frequencies, the non-uniform impacts damped the bar's response to a level comparable to that of the tuned mass damper.

The nature of vibro-impacts changes significantly when friction is included, for when the gap is low and the force is high – see Fig. 3(d). From there being six types of vibro-impacts without friction, there are now four different types of solutions. These include cases with no impacts, a case of sticking behavior, and cases of two and more symmetric impacts. In general, the response characteristics for the low gap level are like those observed for the higher gap (see Fig. 3(b)). The only major notable difference is that for higher frequency ratios, despite the vibro-impacts being of the two symmetric impacts per cycle type, there is no reduction in the RMS levels in comparison to the solid bar's response. Since response characteristics for cases with no impacts, sticking, and two and more symmetric impacts were already shown, those are not shown again.

Our model-based parametric analysis of vibro-impacts under harmonic excitations concludes here. In general, we observed the nature of vibro-impacts to be strongly dependent on friction, the excitation level, the excitation frequency, and on the gap between the free mass and the walls of the bar. Families of solutions for vibro-impacts include multiple symmetric and asymmetric impact cases, no impact cases, as well as cases with ball sticking to a wall and cases with the ball exhibiting non-uniform modulated response. Our analysis also reveals that friction changes the nature of vibro-impacts resulting in a transition of response from one solution type to others. We next turn our attention to the boring process being influenced by friction in the impact damper.

Machining Stability Analysis

This section discusses the response of the impact-damped bar to regenerative cutting forces. In general, regenerative chatter is characterized by large amplitude limit cycle oscillations of the bar, which, in a way, is that the free-mass experiences when it repeatedly impacts the two side walls. To evaluate the role of the vibro-impacts of the free mass on the vibration behaviour of the bar, we solve Eq. (4) by setting the forcing function equal to the regenerative cutting force. The force hence becomes a function of the material being cut, the depth of cut, and the instantaneous chip thickness, which in turn is a function of mean chip thickness and the spindle period(s). For assumed cutting of Aluminium with a mean chip thickness (feed) of 0.1 mm/rev, we characterize how the response changes for changing depths of cuts and spindle periods (speeds).

We establish a simulation grid in which we discretize the speed from 900 to 1600 RPM in increments of 50. Likewise, for the depth of cut, we initialize it at a minimum value of 0.01 mm and increase it in steps of 0.01 mm until the system consistently exhibits chatter across multiple successive increments. The first instance of instability is classified as the limiting boundary of stable depth of cut at the speed being investigated. We classify chatter as the case in which the cutting force instantaneously goes to zero. This condition is met when the response of the bar is large enough such that the instantaneous chip thickness becomes negative, i.e., a condition in which the tool leaves the cut that results in the forces becoming zero. This condition corresponds to cutting-edge contact loss and is adopted here as the instability indicator since it represents a clear physical threshold leading to intermittent tool–workpiece engagement and unacceptable machining conditions.

As for the case of harmonic excitation, with regenerative excitations too, we characterize how the machining stability is influenced by changing gaps and by the inclusion of friction. Results with a gap of 0.5 mm are shown in Fig. 4 and results with a gap of 0.1 mm are shown in Fig. 5. In each figure, we show the stability boundary as well as what the response and cutting forces look like for representative stable and unstable cuts with and without friction. We also benchmark stability with that of a solid boring bar and a tuned mass damped boring bar – parameters of which were

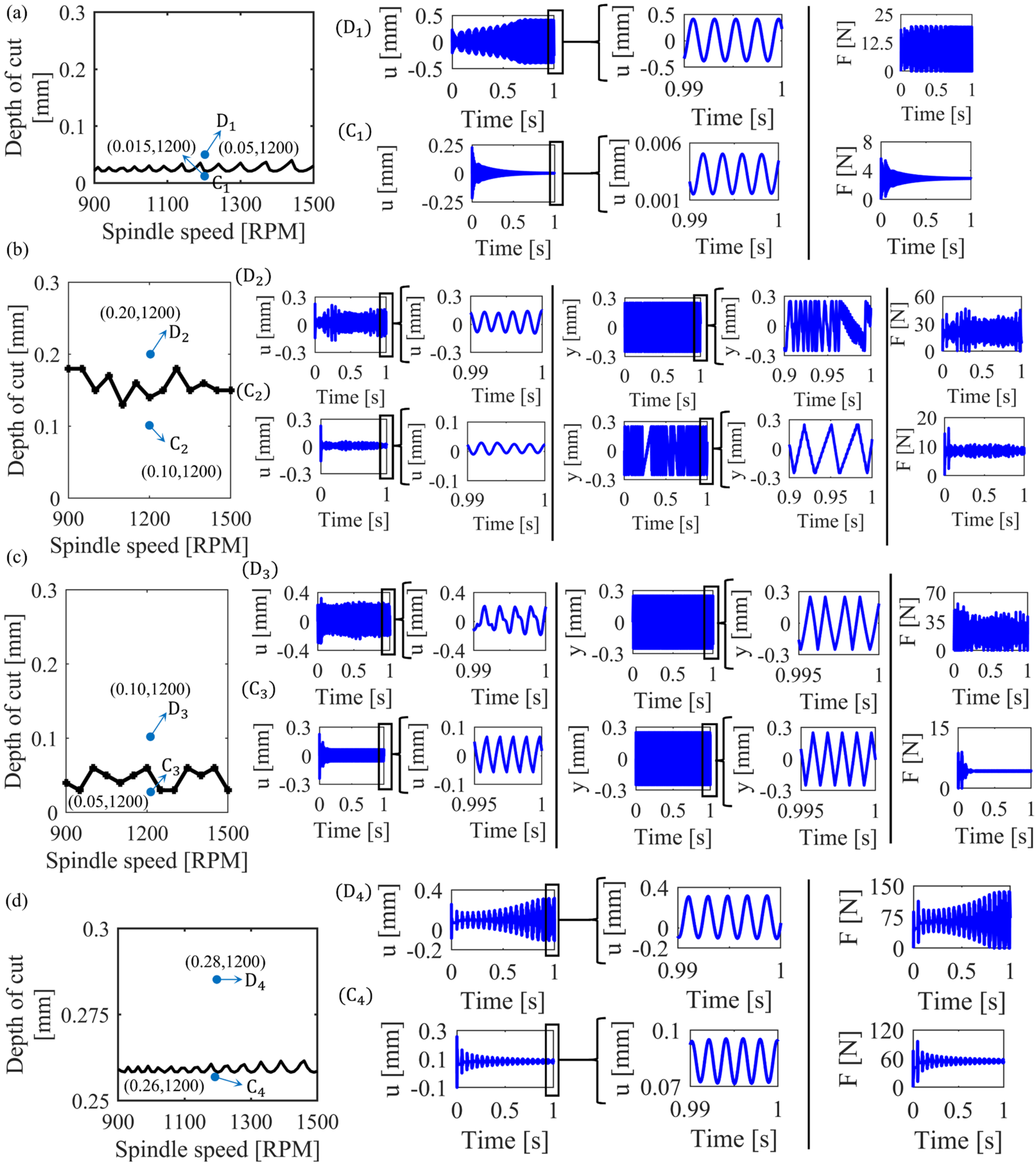

Fig. 4 Stability lobe diagrams for (**a**) solid bar, (**b**) impact-damped bar without friction, (**c**) with friction for the gap of 0.5 mm, and (**d**) bar with tuned mass damper. Points $C_1 - C_4$ and $D_1 - D_4$ indicate stable and unstable cutting conditions, respectively. The corresponding time histories of bar displacement and cutting force on the right illustrate the system response under these conditions

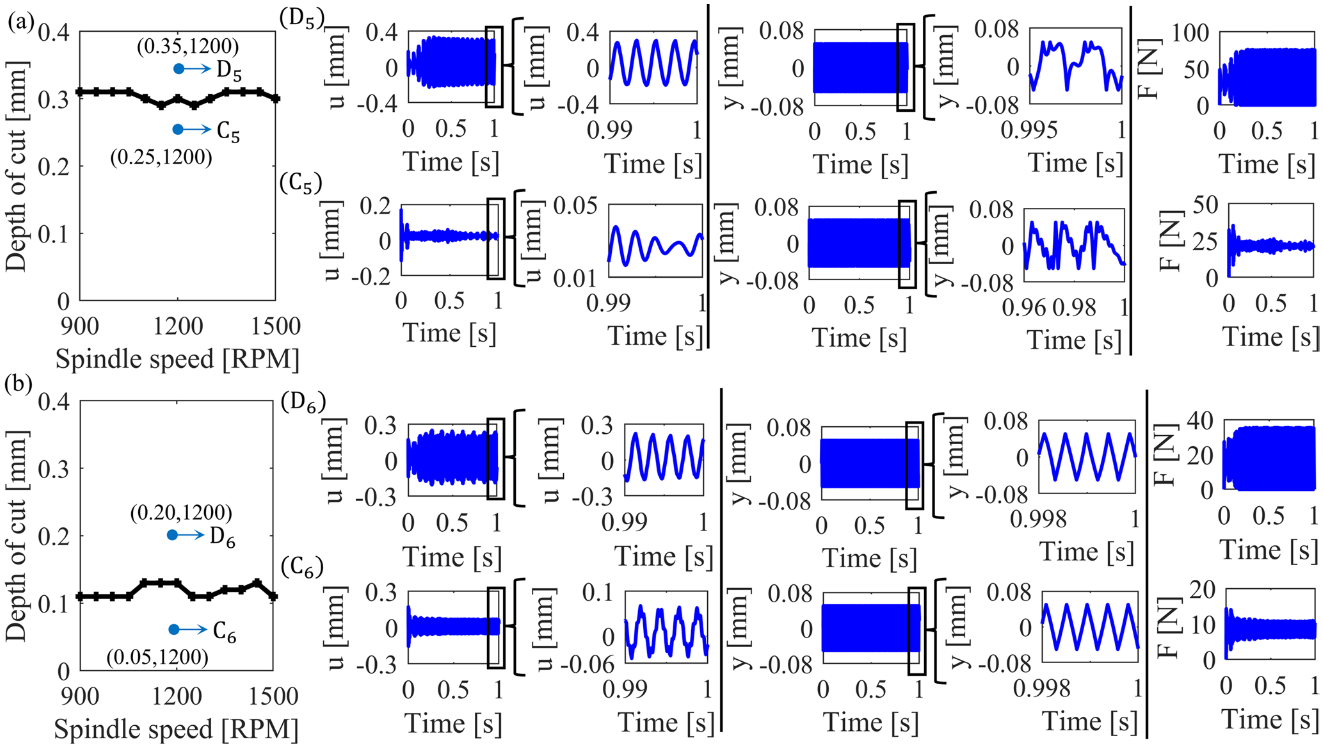

Fig. 5 Stability lobe diagrams for (**a**) impact-damped bar without friction, and (**b**) with friction for the gap of 0.1 mm. Points $C_5 - C_6$ and $D_5 - D_6$ indicate stable and unstable cutting conditions, respectively. The corresponding time histories of bar displacement and cutting force on the right illustrate the system response under these conditions

the same as those listed above. For all analyses herein too, we take the bar and the ball to be stationary at time, $t = 0$ and also assume the ball is centered in the cavity at the start of simulations. Stability being influenced by a change of initial conditions and by a change in the free mass is presented in the 'Discussions' section.

The stability boundary of the solid bar is shown in Fig. 4(a). The solid black line represents the limiting depth of cut, separating stable cutting conditions from unstable (chatter) regions. The response for two representative cutting conditions, one stable (C_1) and one unstable (D_1), is presented. In the stable case, the response decays following an initial transient and subsequently attains a steady state characterized by small cutting forces. In contrast, the unstable case exhibits large-amplitude vibrations typical of chatter. These vibrations result in the cutting force periodically reducing to zero when the tool leaves the workpiece.

For the impact-damped bar without friction being considered in the model, the stability boundary is shown in Fig. 4(b). And, as is evident, the minimum chatter-free depth of cut, increases from 0.021 mm for the solid bar to 0.13 mm, a significant 519% improvement. A representative example of an unstable (D_2) cutting condition shows the response to exhibit modulations as well as limit cycle oscillations. The cutting forces too are large. In part due to the depth of cut being high, and also because of the vibratory response causing the forces to grow. The tool-out-of-cut effect is evident from the forces becoming zero at several time instants. In contrast to this, forces for the stable (C_2) cut do not fall to zero at any time instant. Interestingly, the response, in the stable case does not exhibit the periodic steady state behavior like was observed for a stable cut with the solid boring bar. The response with the impact damper instead is strongly modulated on account of the vibro-impacts between the ball and the bar, with the ball undergoing nonuniform impacts at several instants in time. Despite not exhibiting periodicity, we still classify such cases as stable because the force does not ever fall to zero – the criterion we use to classify an unstable cut. Moreover, the tool-tip vibration amplitude is about 0.03 mm, which is well below the depth of cut of 0.1 mm; therefore, the resulting chip thickness modulation is limited, and the surface quality is not expected to be adversely affected.

The inclusion of friction in the impact-damped bar significantly reduces the stability boundary- see Fig. 4(c). The minimum chatter-free depth of cut with friction included increases slightly to about 0.03 mm compared to the solid bar. The response with friction remains strongly modulated for the stable (C_3) and unstable (D_3) cases, and additionally exhibits limit cycle oscillations with the tool jumping out of cut effect for the unstable case. Furthermore, both the depth of cut and tool-tip displacement for C_3 are large, which may consequently lead to substantial chip thickness modulation and poorer surface finish.

To benchmark the performance of the impact-damped bar, Fig. 4(d) shows the stability boundary achievable with a tuned mass damped boring bar. The minimum chatter-free depth of cut for the tuned mass system is 0.26 mm. This is 1138% higher than the stability limit for the solid boring bar, and approximately 100% higher than the frictionless impact-damped boring bar. Representative stable (C_4) and unstable (D_4) response characteristics for this case are like the behaviour observed for the solid boring bar. The tuned mass system is linear, unlike the impact-damped system which is nonlinear. Hence, in the stable case, the response settles to a steady-state behavior. In the unstable case, limit cycle oscillations occur, with time instants at which the forces become zero.

Since the tuned mass system outperforms the impact-damped system when the gap was 0.5 mm, we also present analysis with the gap between the ball and bar being reduced to 0.1 mm. Those results are shown in Fig. 5(a) for the case of friction being ignored, and in Fig. 5(b) for the case of friction being included in the analysis. Since the response of the solid bar and that of the tuned mass system are independent of changing gap, the results from Fig. 4(a) and (d) are not repeated in Fig. 5.

As is evident from the results in Fig. 5(a) that ignores the role of friction, a reduction in the gap from 0.5 mm to 0.1 mm increases the minimum chatter-free depth of cut from 0.13 mm to 0.29 mm. The improvement in the chatter-free depth of cut to 0.29 mm is slightly higher than that possible with a tuned mass system. The lower gap facilitates better exchange of momentum between the bar and the ball and hence results in better damping. However, even in this case, the stable (C_5) response remains strongly modulated. The unstable case (D_5) is also characterized by modulated limit cycle oscillations associated with the tool jumping out of the cut effect.

When friction is included, the minimum chatter-free depth of cut reduces to 0.11 mm from it being 0.29 mm without friction. The 0.11 mm depth of cut is approximately 423% higher than the case of the solid boring bar, but still significantly less than the case of the tuned mass damped system. The response characteristics for both the stable (C_6) and unstable (D_6) cases remain strongly modulated, with the force also going to zero at several time instants in the unstable case.

Our analysis indicates that friction in the impact-damped boring bar has a destabilizing effect on the machining process. For higher gaps between the ball and the bar, we found that the impact-damped bar offers negligible improvement in the cutting stability in comparison to the solid boring bar. And, though for lower gaps, there was an approximate 423% increase in the minimum chatter-free depth of cut, this improvement is nowhere near what is possible with the tuned mass damped system.

Discussions

Since the impact-damped system is nonlinear, we herein discuss the sensitivity of the nature of vibro-impacts to changes in initial conditions, to changes in harmonic forcing excitation amplitude, to changes in mass ratios, to changes in the friction coefficient, and to change in the restitution coefficient. These effects are examined for both harmonic as well as regenerative forcing.

On the role of a change in initial conditions: Sensitivity to changes in initial conditions is analyzed by constructing basins of attraction through systematic variation of initial conditions in the initial-condition space. For the cases shown in Figs. 2 and 3, the basins were generated by varying the initial tool displacement x_0 from −1.5 mm to 1.5 mm using 30 equally spaced values. Similarly, the initial tool velocity v_0 was varied from −1.5 m/s to 1.5 m/s with 30 discrete values, resulting in a total of 900 initial conditions for each operating case. For each initial condition, time-domain simulations were performed for a duration of 2 s. The initial 20% of the response was discarded to remove transient effects, and the steady-state behavior was examined to identify the number and nature of attractors. In addition, a representative initial condition near the attractor was selected to construct the corresponding Poincaré map by sampling the response once every forcing period. The resulting basins of attraction and the associated Poincaré maps are shown in Fig. 6 for three representative cases: without friction when no impact occurs for a harmonic forcing of 10 N, a frequency ratio of 1.01, and a gap of 0.5 mm, shown in Fig. 6(a); with friction when no impact occurs for the same harmonic forcing and frequency ratio, with a gap of 0.5 mm and a friction coefficient of 0.6, shown in Fig. 6(b); and a case with two symmetric impacts for a harmonic forcing of 20 N, a frequency ratio of 1, and a gap of 0.5 mm, shown in Fig. 6(c).

As evident from Fig. 6(a), the basin of attraction does not converge to a fixed point or a periodic orbit such as a limit cycle. Instead, the trajectories evolve toward an irregular attractor, indicating the presence of chaotic dynamics. Furthermore, when the bar is initiated from rest, an attractor corresponding to a no-impact orbit with displacement in the range of 0.3 mm appears; however, it vanishes and transitions to a non-uniform impact orbit as the displacement is slightly increased. Since, in Fig. 6(a), the amplitudes of both attractors overlap, the attractor corresponding to the

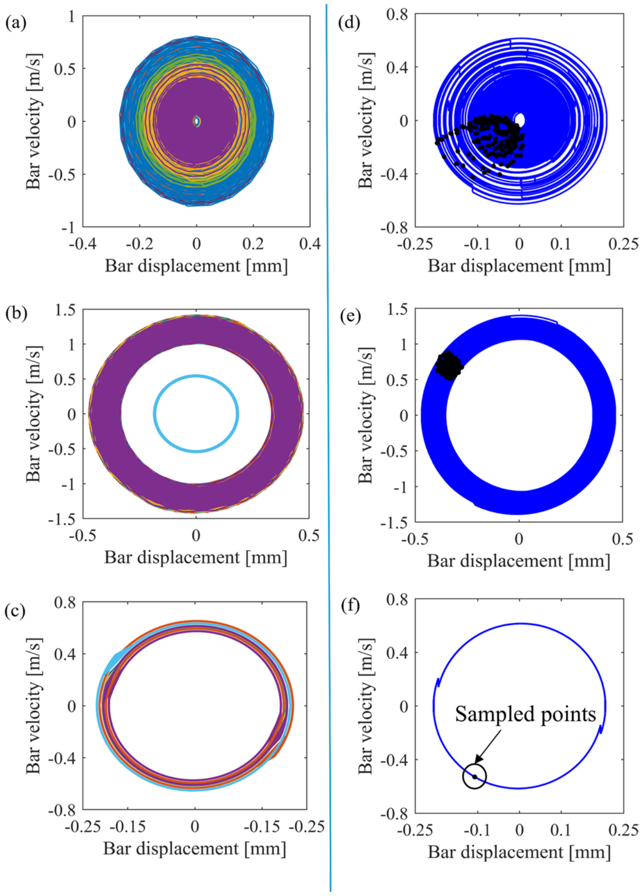

Fig. 6 Basin of attraction (left column) for an impact-damped boring bar under harmonic forcing: **(a)** $F_0 = 10\,\mathrm{N}$, $r = 1.01, \delta = 0.5$ mm, $\nu_{\mathrm{rf}} = 0$ **(b)** $F_0 = 10\,\mathrm{N}$, $r = 1.01, \delta = 0.5$ mm, $\nu_{\mathrm{rf}} = 0.6$ mm, and **(c)** $F_0 = 20\,\mathrm{N}$, $r = 1.0, \delta = 0.5$ mm, $\nu_{\mathrm{rf}} = 0$. Poincaré map (right column) for an impact-damped boring bar: **(d)** $x_0 = 0.5$ mm, and $v_0 = 0.5$ m/s, **(e)** $x_0 = 1.0$ mm, and $v_0 = 1.0$ m/s, and **(f)** $x_0 = 0.5$ mm, and $v_0 = 0.5$ m/s

no-impact orbit is not clearly visible. To further examine the nature of the response, a representative initial condition was selected for the chaotic attractor and the corresponding Poincaré map is constructed, as shown in Fig. 6(d). The sampled points are scattered over a region of the phase space rather than lying on a finite set of discrete points or on a smooth closed curve because the ball experiences nonuniform impacts, which is characteristic of chaotic motion.

Similarly, the case shown in Fig. 6(a) was examined with friction, and the corresponding basin of attraction is shown in Fig. 6(b). Two attractors are observed: a closed orbit corresponding to no-impact motion when the initial bar displacement is small, typically below 1 mm, and a thick annular region in phase space where the trajectories appear irregular. When the initial displacement exceeds 1 mm, the response transitions to this annular attractor. The corresponding Poincaré map, shown in Fig. 6(e), exhibits densely scattered sampled points in phase space due to the nonuniform impact motion of the ball, indicating chaotic dynamics.

Next, the case corresponding to two symmetric impacts per cycle of the bar motion, shown earlier in Fig. 3(a), was considered. In this case, the response forms a closed orbit in phase space, as shown in Fig. 6(c). The corresponding Poincaré map shown in Fig. 6(f) consists of a single point, highlighted by a circle, indicating a periodic response. The basin of attraction further reveals multiple closely spaced closed orbits, and depending on the initial conditions, the solution converges to one of these nearby periodic orbits. For the non-uniform impact motion, basing of attraction is characterized by chaotic attractor only.

All other types of vibro-impacts such as non-uniform impacts, sticking, and multiple symmetric and asymmetric impact types were observed not to change their vibro-impacting character if/when the initial conditions changed. In all such cases, even though the vibro-impacting character remains unchanged, we observed small changes in the RMS levels of vibrations of the bar. However, these small changes were insignificant. For the case of regenerative excitations, since the response with the original initial conditions was already strongly modulated and non-uniform, changes in initial conditions were not observed to have any significant change in the response characteristics. Moreover, cases that were stable or unstable with the original initial conditions remained so even with a change in initial conditions. These observations indicate that the vibro-impact behavior and response characteristics of impact-damped boring bars are generally robust to changes in initial conditions. The only exception was observed for harmonic forcing when the ball undergoes a no-impact motion, with or without friction, when both the bar and the ball are initially at rest. In this case, a change in the initial conditions introduces non-uniform impacts in ball's motion, leading to a corresponding change in the bar's response characteristics.

On the role of a change in harmonic forcing amplitude: A change in the harmonic forcing amplitude is also investigated through a bifurcation analysis by varying the excitation force from 5 N to 50 N in increments of 1 N, where the upper limit of 50 N was chosen since larger force levels are impractical under stable cutting conditions in boring operations. For each force level, the steady-state behavior was characterized using stroboscopic Poincaré sampling at the forcing period. To capture possible multistability, the excitation force was varied gradually in both forward and backward directions, with the final state of each simulation used as the initial condition for the next step. This continuation procedure enables the identification of different attractors that may coexist at the same forcing level and reveals the dependence of the steady-state response on the parameter variation path. The resulting bifurcation diagrams are shown in Fig. 7 for four representative cases corresponding to gaps of 0.1 mm and 0.5 mm when the bar is excited at its natural frequency, without and with friction for a carbide damper ball.

In the first case shown in Fig. 7(a), a single point appears in the Poincaré section for each forcing level, indicating a periodic response whose displacement amplitude increases steadily with increasing forcing amplitude. In contrast, in the second case, where the gap is increased from 0.1 mm to 0.5 mm as shown in Fig. 7(b), multiple points appear in the bifurcation plot at a forcing level of 10 N, indicating that the response is no longer periodic and may be chaotic. This case corresponds to the non-uniform impacting motion observed in Fig. 2(a). However, for forcing levels greater than 10 N, periodic solutions reappear.

When friction is included, a markedly different behavior is observed. In particular, a sudden jump in the displacement amplitude occurs near a forcing level of approximately 19 N, as shown in Fig. 7(c). At this forcing level, two different attractors coexist: the forward-sampled displacement is approximately −0.077 mm, whereas the backward-sampled displacement is approximately −0.42 mm, indicating the presence of a large-amplitude attractor at 19 N. However, at 20 N, the response settles again to a smaller-amplitude attractor, where a single point is observed corresponding to the onset of sticking, as also seen in Fig. 3(d). As the forcing level increases beyond 20 N, the response consistently settles onto the larger-amplitude attractor. In the case shown in Fig. 7(d), the response exhibits chaotic behavior in the forcing range of approximately 17–28 N, and beyond this range another chaotic attractor with significantly larger amplitude emerges for forcing levels above approximately 33 N. Overall, the analysis reveals that the response can transition between chaotic and periodic attractors, and vice versa, as the forcing amplitude is varied.

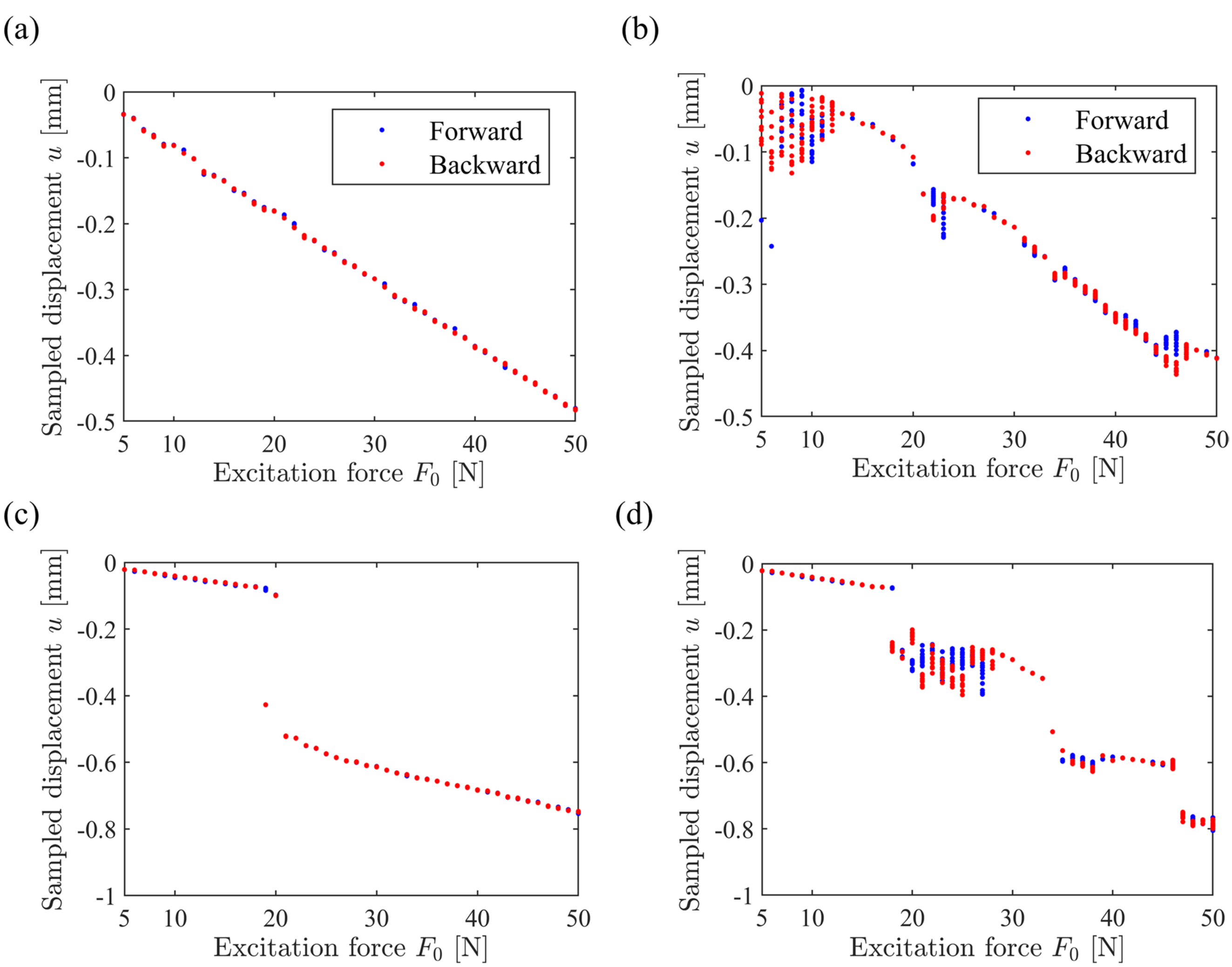

Fig. 7 Bifurcation diagram for impact-damped bar at the resonance for: **(a)** $\delta = 0.1$ mm, $\nu_{\mathrm{rf}} = 0$, and **(b)** $\delta = 0.5$ mm, $\nu_{\mathrm{rf}} = 0$, **(c)** $\delta = 0.1$ mm, $\nu_{\mathrm{rf}} = 0.6$ mm, **(d)** $\delta = 0.5$ mm, and $\nu_{\mathrm{rf}} = 0.6$ mm

Now we discuss how the gap influences the bifurcation behavior. For the case without friction, comparison of Fig. 7(a) and (b) shows that for a gap of 0.1 mm in Fig. 7(a), the sampled displacements for forcing levels of 10 N, 20 N, and 30 N are approximately −0.08 mm, −0.18 mm, and −0.28 mm, respectively, indicating periodic responses. When the gap is increased to 0.5 mm as shown in Fig. 7(b), the response for 10 N changes to non-uniform impacts, producing multiple sampled displacements between −0.024 mm and −0.1 mm, indicating chaotic behavior. For 20 N and 30 N, the sampled displacements are approximately −0.11 mm and −0.21 mm, respectively, again corresponding to periodic responses. These results indicate that increasing the gap slightly reduces the vibration amplitude at higher forcing levels while promoting non-uniform impacts and chaotic responses at lower forcing levels.

For the case with friction, comparison of Fig. 7(c) and (d) shows that for a gap of 0.1 mm in Fig. 7(c), the sampled displacements for 10 N, 20 N, and 30 N are approximately −0.04 mm, −0.098 mm, and −0.6 mm, respectively, all corresponding to periodic responses. When the gap is increased to 0.5 mm as shown in Fig. 7(d), the response for 10 N remains periodic with a sampled displacement of approximately −0.04 mm. For 20 N, the ball undergoes non-uniform impacts, producing sampled displacements between −0.2 mm and −0.3 mm, indicating chaotic behavior. For 30 N, the sampled displacement is approximately −0.28 mm, corresponding to a periodic response. These observations further indicate that in the presence of friction, increasing the gap can reduce the vibration amplitude of the boring bar at larger excitation forces and also promotes change in response from periodic to chaotic.

On the role of a change in mass ratio: A change in mass ratio, arising from replacing the free mass material from carbide to steel, was observed to alter the RMS levels during forced excitation. It also affected the minimum chatter-free depths of cut in the case of regenerative excitations. The RMS trends remained consistent for both mass ratios, namely a leftward shift in the absence of friction and a rightward shift when friction was included. However, replacing the carbide ball with a steel one generally led to a slight increase in the RMS levels. Thus, the overall performance was inferior when a steel ball was used. We also observed the nature and type of vibro-impacts to change with a change in mass ratios. For example, in some cases, we observed cases with non-uniform impacts to transition to cases of no-impacts. And, in other cases, we observed symmetric vibro-impacts to transition to asymmetric impacts when the ball changed from being carbide to steel. Furthermore, under different initial conditions, the change in the nature of the response and the impact patterns remains consistent with that of the carbide ball; specifically, no-impact cases exhibit impacts, while other response types remain largely unchanged. For the case of regenerative excitations, a change to the steel ball was observed to lower the minimum chatter-free depth of cut by as much as 15%. Since the response characteristics were already strongly modulated for all stable and unstable cases, a change to the steel ball did not change that behavior. The increase in the RMS levels and the reduction in the minimum chatter-free depths of cut with the steel ball can be explained by the steel ball being lighter and hence resulting in smaller momentum exchanges during impacts. It may also be noted that carbide is already a dense (heavy) material, and therefore impact dampers with masses larger than that of the carbide were not considered in the present analysis.

On the role of a change in friction coefficient: Sensitivity to change in friction coefficient is also examined, as it was found to destabilize the cutting process and significantly reduce the machining stability boundaries. To investigate this further, we considered the case shown in Fig. 4(c), where stable and unstable responses at 1200 RPM are presented for depths of cut of 0.05 mm and 0.10 mm with a friction coefficient of 0.6 mm. Additional simulations were performed by varying the friction coefficient from 0.2 to 0.8 mm while considering depths of cut between 0.05 and 0.10 mm at the same spindle speed. The results show that for lower friction coefficients such as 0.2 and 0.4 mm, cutting becomes unstable even for cases that are stable at 0.6 mm, while stability is recovered when the friction coefficient exceeds approximately 0.5 mm. This trend is also reflected in the total mechanical energy, computed as the sum of kinetic and potential energies using the tool-tip displacement and velocity, which decreases significantly as the response approaches stability with increasing friction coefficient. For larger depths of cut above 0.06 mm, for example at 0.08 mm, the response remains unstable when the friction coefficient is below or equal to 0.6 mm but can regain stability at higher friction levels such as 0.8 mm, whereas depths of cut of 0.10 mm and above remain unstable regardless of the friction coefficient. A similar trend is observed for the case shown in Fig. 5(b), where lower friction coefficients lead to instability in cases which are stable for friction coefficient of 0.6 mm and stability is achieved only when the friction coefficient exceeds approximately 0.5.

For harmonic forcing, the analysis shows that the inclusion of friction may lead to no-impact motion when the bar is excited at or below its natural frequency, as shown in Figs. 2 and 3. However, smaller friction coefficients in the range of 0.2–0.4 are found to induce nonuniform impacts even under these conditions, whereas no-impact behavior is observed for a friction coefficient of 0.6. For the other cases in Figs. 2 and 3, where inclusion of friction leads to symmetric impacts and/or asymmetric and/or sticking motion, variations in the friction coefficient do not produce significant changes in the response.

On the role of a change in coefficient of restitution: The influence of changing the coefficient of restitution e was also investigated by considering $e = 0.6$ and $e = 0.8$, i.e., values lower and higher than that reported in the original manuscript. Values lower than 0.6 were not considered because the bar and impacting mass are typically made of hard materials, while values higher than 0.8 were not explored since real systems do not exhibit perfectly elastic collisions. It was observed that when the nature of impacts were symmetric, and/or asymmetric, and/or there were no-impact, a change in e does not alter the nature of impacts, whereas for nonuniform impact motion, a slight change in the RMS displacement was observed.

The present analysis is based on time-domain simulations with event detection. A more rigorous analysis of impacting periodic solutions could be achieved by formulating the problem as a multi-point boundary value problem and employing numerical continuation techniques to systematically track periodic impacting orbits and their bifurcations, as demonstrated in Iklódi et al. [5]. Although such an approach is important for a mathematically systematic analysis of vibro-impact systems, it is beyond the scope of the present study.

Conclusion

This study examined the influence of friction on vibro-impact dynamics in an impact-damped boring bar and its consequences for machining stability. Through a detailed nonlinear, model-based parametric analysis, we demonstrated that friction plays a decisive role in shaping the families of vibro-impact solutions, including symmetric and asymmetric impacts, sticking, non-uniform modulated responses, and no-impact cases. Friction was shown to retard the motion of the free mass in case of regenerative forcing, inhibiting momentum transfer and, in turn, reducing damping effectiveness, and thereby reducing the chatter-free limiting stable depth of cut during boring processes. Through our analysis, we observed that smaller gap values, together with a relatively large impact mass tend to enhance the damping performance of the vibro-impact system.

Sensitivity studies revealed that, despite the inherent nonlinearity and non-smooth nature of the system, the vibro-impact responses are generally robust to changes in initial conditions, except for the no-impact motion observed under harmonic forcing. Variations in harmonic forcing showed that, when friction is considered, two different attractors can exist, one with smaller amplitude and the other with larger amplitude. Changes in the mass ratio produced more pronounced effects on the system response. Furthermore, changes in the friction coefficient indicated that smaller values of the coefficient can destabilize machining operations that remain stable for larger coefficient values. In contrast, changes in the coefficient of restitution were found to have no significant effect on the response or impact characteristics. Future work should extend these insights experimentally to validate transition phenomena and quantify frictional effects under realistic surface conditions.

Acknowledgements Authors gratefully acknowledge support from the Government of India's Department of Science & Technology's grant on technology development via grant number DST/TDT/AM/2022/148.

Declarations

Competing interest The authors declare that they have no known competing financial interests or personal relationships that could have appeared to influence the work reported in this paper.

References

1. Munoa J, Beudaert X, Dombovari Z, Altintas Y, Budak E, Brecher C (2016) Chatter suppression techniques in metal cutting. CIRP Ann - Manuf Technol 65:785–808. https://doi.org/10.1016/j.cirp.2016.06.004
2. Thomas MD, Knight WA, Sadek MM (1974) Impact Damper As a Method of Improving Cantilever Boring Bars. Am Soc Mech Eng 859–866. https://doi.org/10.1115/1.3438693
3. Ema S, Marui E (2000) Suppression of chatter vibration of boring tools using impact dampers. Int J Mach Tools Manuf 40:1141–1156. https://doi.org/10.1016/S0890-6955(99)00119-4
4. Gourc E, Seguy S, Michon G, Berlioz A, Mann BP (2015) Quenching chatter instability in turning process with a vibro-impact nonlinear energy sink. J Sound Vib 355:392–406. https://doi.org/10.1016/j.jsv.2015.06.025
5. Iklodi Z, Barton DAW, Dombovari Z (2022) Bi-stability induced by motion limiting constraints on boring bar tuned mass dampers. J Sound Vib 517:116538. https://doi.org/10.1016/j.jsv.2021.116538
6. Patel A, Law M, Wahi P (2023) Vibration suppression of a slender boring bar by an impact damper. Manuf Technol Today 22:14–19. https://doi.org/10.58368/MTT.22.4.2023.14-19
7. Patel A, Law M, Wahi P (2024) Damping chatter vibrations of a boring bar by an integrated impact damper BT - Proceedings of the 15th international conference on vibration problems. In: Sassi S, Biswas P, Naprstek J, editors., Singapore: Springer Nature Singapore, pp. 305–14. https://doi.org/10.1007/978-981-99-5922-8_28
8. Masri SF (1970) General Motion of Impact Dampers. J Acoust Soc Am 47:229–237. https://doi.org/10.1121/1.1911470
9. Bapat CN, Sankar S (1985) Single unit impact damper in free and forced vibration. J Sound Vib 99:85–94. https://doi.org/10.1016/0022-460X(85)90446-8

10. Cheng CC, Wang JY (2003) Free vibration analysis of a resilient impact damper. Int J Mech Sci 45:589–604. https://doi.org/10.1016/S0020-7403(03)00116-4
11. Chabrier R, Chevallier G, Foltête E, Sadoulet-Reboul E (2022) Experimental investigations of a vibro-impact absorber attached to a continuous structure. Mech Syst Signal Process 180:109382. https://doi.org/10.1016/j.ymssp.2022.109382
12. Yalamati HC, Patel A, Bhoge J, Wahi P, Law M (2024) Experimental analysis of the dynamics of an impact damped boring bar. Int Conf Precision, Micro. Meso Nano Eng (COPEN-13)
13. Gendelman OV, Alloni A (2016) Forced System with Vibro-impact Energy Sink: Chaotic Strongly Modulated Responses. Procedia IUTAM 19:53–64. https://doi.org/10.1016/j.piutam.2016.03.009
14. Den JP, Hartog (1985) Mechanical vibrations. Dover, New York, USA
15. Yadav A, Talaviya D, Bansal A, Law M (2020) Design of chatter-resistant damped boring bars using a receptance coupling approach. J Manuf Mater Process. https://doi.org/10.3390/jmmp4020053
16. Sims ND (2007) Vibration absorbers for chatter suppression: A new analytical tuning methodology. J Sound Vib 301:592–607. https://doi.org/10.1016/j.jsv.2006.10.020
17. Ozlu E, Budak E (2007) Analytical modeling of chatter stability in turning and boring operations - Part I: Model development. J Manuf Sci Eng Trans ASME 129:726–732. https://doi.org/10.1115/1.2738118
18. Tlustý J (1999) Manufacturing processes and equipment. Prentice-Hall
19. Wei-ming Y, Bao-shun W, Hao-xiang H (2019) Research of mechanical model of particle damper with friction effect and its experimental verification. J Sound Vib 460:114898. https://doi.org/10.1016/j.jsv.2019.114898
20. Güttler C, Heißelmann D, Blum J, Krijt S (2012) Normal Collisions of Spheres: A Literature Survey on Available Experiments. ArXiv Prepr ArXiv12040001. https://doi.org/10.48550/arXiv.1204.0001
21. Patel A, Yadav A, Law M, Bhattacharya B, Wahi P (2022) Damped Chatter Resistant Boring Bar Integrated with an Absorber Working in Conjunction with an Eddy Current Damper. J Vib Eng Technol. https://doi.org/10.1007/s42417-022-00684-9
22. Athanasouli C, Yurchenko D, Kuske R (2025) Analysis of Dry Friction Dynamics in a Vibro-Impact Energy Harvester. ArXiv:1–48. https://doi.org/10.48550/arXiv.2502.12288
23. Youssef B, Karoui AY, Leine RI (2025) The effect of friction on the dynamics of targeted energy transfer by symmetric vibro-impact dampers. ArXiv 250504420:1–55. https://doi.org/10.48550/arXiv.2505.04420
24. He B, Ouyang H, He S, Ren X (2017) Stick-slip vibration of a friction damper for energy dissipation. Adv Mech Eng 9:1–13. https://doi.org/10.1177/1687814017713921
25. Bhoge J, Kumar M, Charan H, Patel A, Law M (2024) New vision-based evidence of the nature of vibro- impacts in an impact-damped boring bar. Proc 20th Int Conf Precis Eng (ICPE 2024):23–7
26. Masri SF (1966) On the Stability of the Impact Damper. J Appl Mech 33:586–592. https://doi.org/10.1115/1.3625125